CHEMISTRY OF MATERIALS
Cite This: Chem. Mater. 2018, 30, 1762−1768
Article
pubs.acs.org/cm

Covalent Organic Framework with Frustrated Bonding Network for Enhanced Carbon Dioxide Storage

Qiang Gao,[†,‡] Xing Li,[‡] Guo-Hong Ning,[‡] Hai-Sen Xu,[‡] Cuibo Liu,[†,‡] Bingbing Tian,[†,‡] Wei Tang,[∥] and Kian Ping Loh*[,†,‡]

[†]SZU-NUS Collaborative Innovation Center for Optoelectronic Science & Technology, Key Laboratory of Optoelectronic Devices and Systems of Ministry of Education and Guangdong Province, College of Optoelectronic Engineering, Shenzhen University, Shenzhen 518060, China

[‡]Department of Chemistry, Centre for Advanced 2D Materials (CA2DM), National University of Singapore, 3 Science Drive 3, Singapore 117543, Singapore

[∥]Institute of Materials Research and Engineering, A*STAR, 2 Fusionopolis Way, Innovis, Singapore 138634, Singapore

Supporting Information

ABSTRACT: Two-dimensional covalent organic framework (COF) materials can serve as excellent candidates for gas storage due to their high density of periodically arranged pores and channels, which can be tethered with functional groups. However, post-functionalization tends to disturb the structure of the COF; thus, it is attractive to develop synthetic approaches that generate built-in functionalities. Herein, we develop a new strategy for the construction of 2D-COFs with built-in, unreacted periodic bonding networks by solvent-directed divergent synthesis. Tetraphenylethane (TPE), which combines both π-rigidity for stacking and rotational flexibility, is selected as the central core for COF construction. By solvent control, two distinct COF structures could be constructed, arising from a [4 + 4] condensation pathway (TPE-COF-I) or an unusual [2 + 4] pathway (TPE-COF-II). TPE-COF-II contains unreacted linker units arranged around its pores and shows greatly enhanced carbon dioxide adsorption performance (23.2 wt %, 118.8 $cm^3\ g^{-1}$ at 1 atm, 273 K), which is among the best COF materials for CO_2 adsorption reported to date.

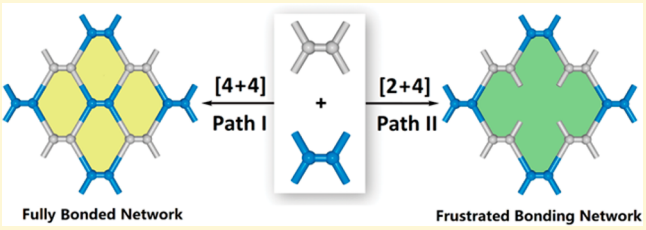

INTRODUCTION

Covalent organic frameworks (COFs) are an emerging class of ordered conjugated organic polymer materials with two-dimensional (2D) layered structures or three-dimensional (3D) networks, which are covalently assembled via various reversible reactions of organic building blocks.[1−7] Porous COF materials showed great potential for application in various fields, such as gas storage,[8−15] heterogeneous catalysis,[16−20] chemical sensors,[21−23] separation,[24,25] drug delivery,[26,27] energy conversion, and storage.[28−31] Faced with a continually escalating level of carbon dioxide (CO_2) in the atmosphere, the development of porous materials for efficient CO_2 capture takes on an ever increasing level of urgency.[32,33] Due to its combination of properties such as low density, high porosity, and thermal stabilities, COFs can act as excellent candidates for CO_2 capture[8,9] if functionalities can be introduced into the pores.

In general, it is believed that the architectures of 2D-COFs are dictated by the symmetries of the building units, and thus reticular chemistry and topology analysis allow predictable products in 2D-COF synthesis. Research on 2D-COF generally involves the preparation of various precursor monomers with different symmetries and the compositional tuning of these monomers and their post-modification;[1−8] less attention has been focused on developing structural variants of the topologically predicted 2D-COFs via tuning the reaction conditions (Figure 1).

Unlike metal organic frameworks whose structures can be easily controlled through the modulation of reaction conditions (i.e., solvent, temperature, and crystallization rate),[34,35] reaction conditions have not been sufficiently exploited by past researchers to modify the structure of 2D-COFs. This is because highly rigid building units are usually chosen to facilitate the crystallization via $\pi-\pi$ stacking, which makes the COF growth condition less sensitive to the environment. One question we raise is whether structural variants of the monostructural 2D-COFs can be achieved if less rigid building units are utilized in the synthesis. To answer this question, we have selected tetraphenylethane (TPE)-based building units[36−41] to investigate the possibility of constructing 2D-COFs with diverse structures, since they combine π-rigidity for stacking and rotational flexibility for geometry self-modulation (Figure 1b). Due to their lower rigidity, the phenyl rings in TPE can have various torsion angles, and the bond angles of the

Received: January 10, 2018
Revised: February 13, 2018
Published: February 13, 2018

DOI: 10.1021/acs.chemmater.8b00117
Chem. Mater. 2018, 30, 1762−1768

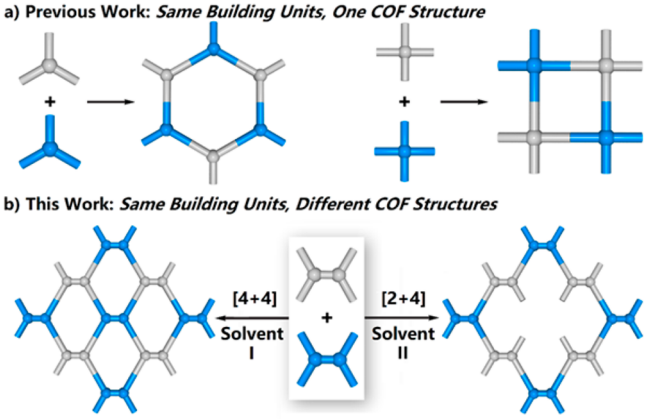

Figure 1. Strategy for construction of COFs using identical starting building units. (a) Previous 2D-COFs materials synthesized have only one fixed COF structure. (b) Our solvent-directed strategy for diverse construction of 2D-COFs with two kinds of COF structures, either fully bonded or frustrated-bonding structures.

carbon in the central olefin bonds with respect to the pendant rings are also variable,[36−38] thereby providing possibilities for different stacking geometries or reaction pathways in 2D-COFs synthesis.

In this study, we demonstrate that an unusual [2 + 4] structural variant of the normal [4 + 4] TPE-COFs can be derived from identical TPE-based precursors, simply by using different solvents in the reaction. The conventional [4 + 4] pathway leads to TPE-COF-I with fully bonded network (Figure 2a), and an unusual [2 + 4] pathway leads to TPE-COF-II with frustrated bonding network (Figure 2b). More interestingly, TPE-COF-II shows excellent carbon dioxide adsorption performance (23.2 wt %, 118.8 cm^3 g^{-1} at 1 atm, 273 K), which is among the highest CO_2 adsorption capacities reported for COF materials to date.

EXPERIMENTAL SECTION

Synthesis of TPE-COF-I. TPE-4NH_2 (**2**, 19.6 mg, 0.05 mmol) and TPE-4CHO (**1**, 22.2 mg, 0.05 mmol) were placed in a 10 mL Schlenk storage tube, and then the mixture was dissolved in solvent (3 mL of *o*-dichlorobenzene/*n*-butanol, 1:1 v/v). Then, 0.2 mL of aqueous 6 M HOAc was added, and the mixture was degassed by three freeze−pump−thaw cycles. Finally, the tube was sealed via the screw cap, heated at 120 °C in an oven, and left undisturbed for 7 days. The obtained precipitate was then immersed and washed in THF three times. Then the powder was dried at 120 °C under vacuum for 24 h. A yellow powder was obtained in 87% isolation yield. Anal. Calcd for $[C_{56}H_{36}N_4]n$: C, 87.47; H, 5.24; N, 7.32. Found: C, 83.50; H, 6.11; N, 7.07.

Synthesis of TPE-COF-II. TPE-4NH_2 (**2**, 9.8 mg, 0.025 mmol) and TPE-4CHO (**1**, 22.2 mg, 0.05 mmol) were placed in a 10 mL

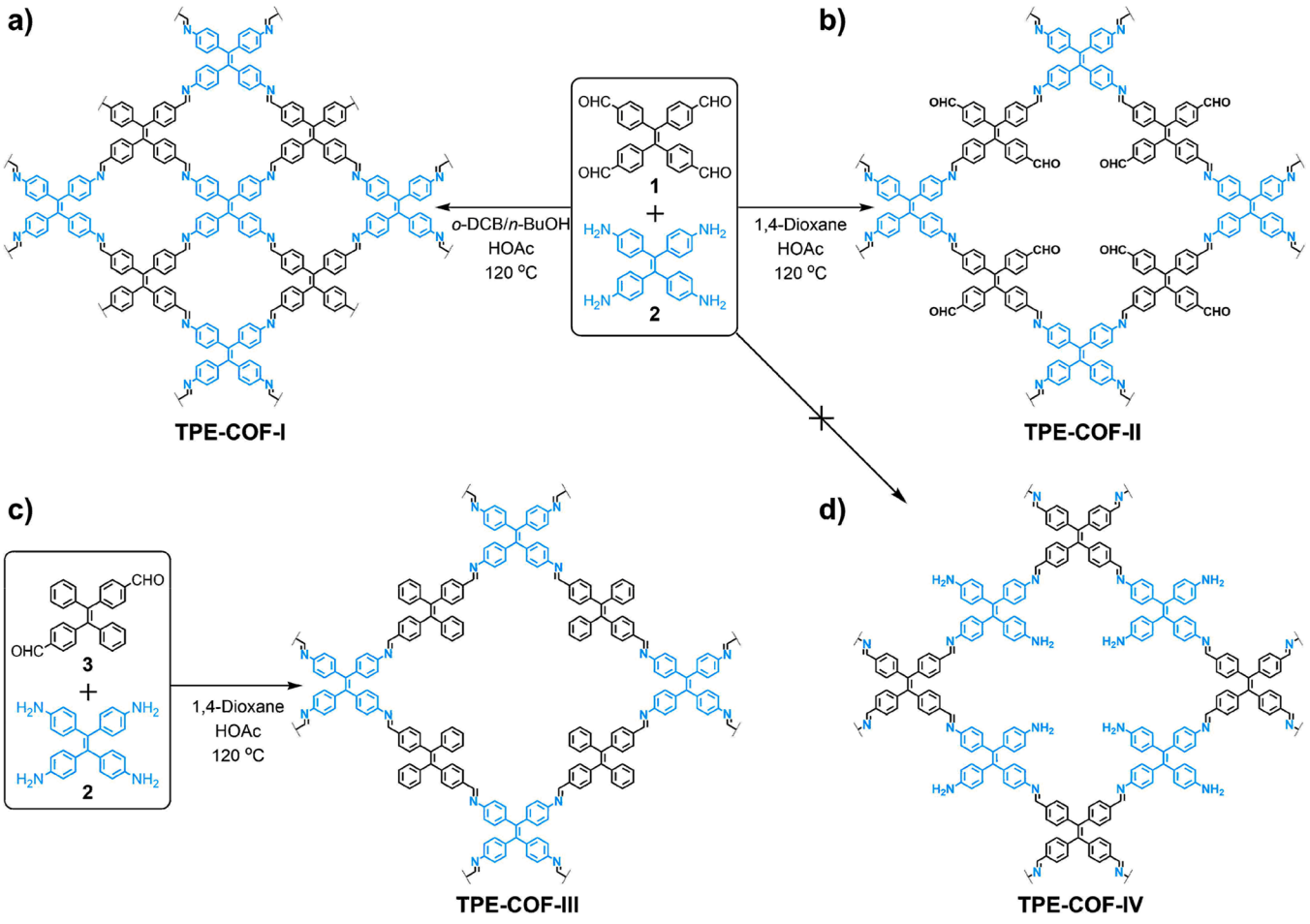

Figure 2. Preparation of TPE-COFs: (a) TPE-COF-I with conventional [4 + 4] pathway. (b) TPE-COF-II with unusual [2 + 4] pathway, with *trans*-position aldehyde groups unreacted. (c) TPE-COF-III with similar structure as TPE-COF-II, for the structure confirmation. (d) Hypothesized TPE-COF-IV structure, with *trans*-position amine group unreacted.

DOI: 10.1021/acs.chemmater.8b00117
Chem. Mater. 2018, 30, 1762−1768

Schlenk storage tube, and then the mixture was dissolved in solvent (3 mL 1,4-dioxane). Then,0.2 mL of aqueous 6 M HOAc was added, and the mixture was degassed by three freeze−pump−thaw cycles. Finally, the tube was sealed via the screw cap, heated at 120 °C in an oven, and left undisturbed for 7 days. The obtained precipitate was then immersed and washed in THF three times. Then the powder was dried at 120 °C under vacuum for 24 h. A yellow powder was obtained in 93% isolation yield. Anal. Calcd for $[C_{86}H_{56}N_4O_4]n$: C, 85.41; H, 4.67; N, 4.63. Found: C, 81.09; H, 5.80; N, 6.34.

Characterization. ^{1}H NMR and ^{13}C NMR spectra were recorded on a Bruker AVIII (400 MHz) NMR spectrometer. Solid-state ^{13}C NMR spectra were recorded on a JEOL ECA400 solid-state NMR spectrometer, 4 mm CPMAS probe, and 100 MHz NMR spectrometer with spin rate as 8000 MHz. Fourier transform infrared spectra were recorded on a Bruker OPUS/IR PS15 spectrometer. TGA characterization was performed on a Discovery TGA thermogravimetric analyzer by heating the samples at 5 °C min^{-1} to 800 °C in a nitrogen atmosphere. Elemental analyses were carried out on an Elementar vario MICRO cube. Powder XRD data were collected on a Bruker D8 Focus Powder X-ray diffractometer using Cu Kα radiation (40 kV, 40 mA) with a step size of 0.032°/min over 2θ range of 2−35° at room temperature. Gas sorption analyses were performed by using Quantachrome Instruments Autosorb-iQ with extra-high pure gases. The samples were activated and outgassed at 120 °C for 8 h before the measurements. The Brunauer−Emmett−Teller (BET) surface area and total pore volume were calculated from the N_2 sorption isotherms at 77 K, and the pore size distribution was calculated based on the N_2 sorption isotherm by using DFT models in the Quantachrome ASiQwin 5.0 software package. SEM imaging of the COF pristine materials was performed using a JEOL JSM-6701F Field Emission. TEM imaging of COF pristine materials was performed on an FEI Titan 80-300 S/TEM (scanning/transmission electron microscope) operated at 200 kV. Crystal Structure modeling and Pawley refinement were carried out using Reflex, a software package for crystal determination from the powder XRD pattern, implemented in BIOVIA Materials Studio modeling version, 2016 (Dassault System).

RESULTS AND DISCUSSION

For divergent synthesis of TPE-COFs, two typical solvent systems with different polarities, such as *o*-dichlorobenzene/*n*-butanol and 1,4-dioxane/mesitylene, are selected. The optimized solvothermal imine condensation of 1,1,2,2-tetrakis(4-formylphenyl)ethane (TPE-4CHO, **1**) and 1,1,2,2-tetrakis(4-aminophenyl)ethane (TPE-4NH$_2$, **2**), with 1:1 ratio in a mixture of *o*-dichlorobenzene/*n*-butanol/HOAc (15:15:2, by vol) or 1,4-dioxane/HOAc (15:1 by vol), is carried out at 120 °C for 7 days and yields highly crystalline TPE-COF-I or TPE-COF-II, which are collected as insoluble yellow powders (Figure 2, see Figure S7−S13 in the Supporting Information).

The formation of imine linkages in TPE-COF-I and TPE-COF-II has been verified by the Fourier transform infrared spectroscopy (FT-IR) and solid-state ^{13}C CP-MAS NMR. The FT-IR spectra of TPE-COF-I and TPE-COF-II exhibit C═N stretching bands at 1624 and 1620 cm^{-1}, respectively, while the TPE model compound (TPE-M) also displays similar C═N vibration bands at 1624 cm^{-1} (Figure S18 in the SI). In addition, they show the characteristic resonance peaks of imine carbons both at 159 ppm in ^{13}C CP-MAS NMR, further evidencing the existence of imine linkages (Figures S14−S17 in the SI). Thermal gravimetric analyses (TGA) of TPE-COF-I and TPE-COF-II under an N_2 atmosphere show that these compounds are thermally stable up to 450 °C (Figure S19 in the SI). Furthermore, scanning electron microscopy (SEM) and transmission electron microscopy (TEM) reveal that they display either coral-like or sheet-like morphology and consist of

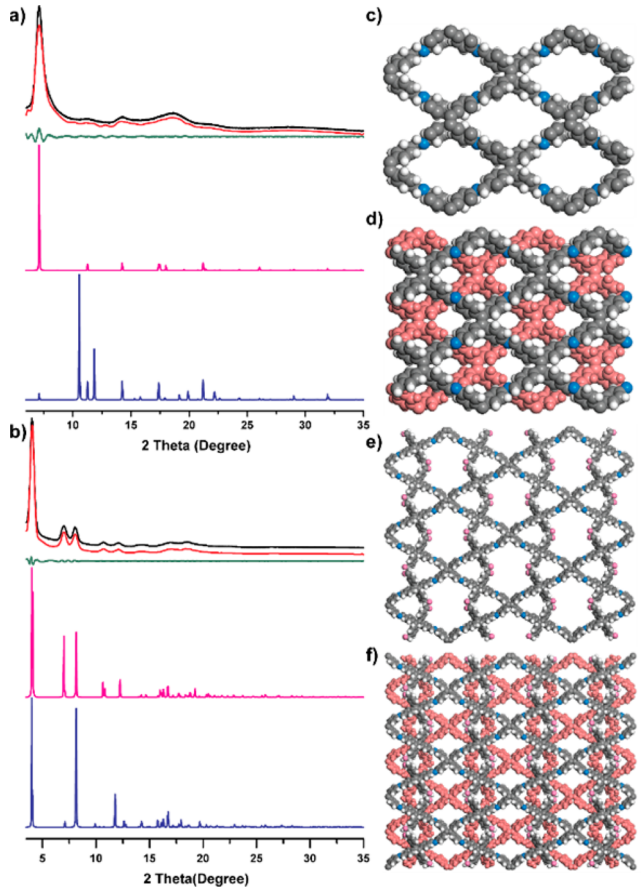

Figure 3. Powder XRD patterns of TPE-COF-I: (a) experimental (black curve), Pawley refined (red curve), difference between the experimental and refined patterns (green curve), and simulated PXRD patterns for eclipsed (pink curve) and staggered structure (blue curve). Simulated crystal structures of (c) eclipsed structure and (d) staggered structure. PXRD patterns of TPE-COF-II: (b) experimental (black curve), Pawley refined (red curve), difference between the experimental and the refined patterns (green curve), and simulated PXRD patterns for eclipsed (pink curve) and staggered structure (blue curve). Simulated crystal structures of (e) eclipsed structure and (f) staggered structure. Views from the *c* axis. C, gray; H, white; N, blue; O, red; lower layer, pink.

uniform porous structure with high crystallinity (Figures S30−S31 and S33−S34 in the SI).

The crystallinity of TPE-COF-I and TPE-COF-II is confirmed by powder X-ray diffraction (PXRD) analyses. The well-defined strong peaks and weak background of experimental PXRD patterns confirm the high crystallinity of TPE-COFs (Figure 3a,b). As shown in Figure 3, TPE-COF-I exhibits intense peaks at 7.11° accompanied by four small and broadened peaks at 11.33°, 14.25°, 18.56°, and 22.06° (Figure S8 in the SI), while TPE-COF-II shows three intense peaks at 4.02°, 6.98°, and 8.06° accompanied by five small peaks at 11.71°, 12.15°, 14.32°, 16.90°, and 18.58° (Figure S10 in the SI), indicating the formation of two completely different structures (Figure S13 in the SI). To further analyze the detailed crystal structures of the obtained TPE-COFs, theoretical simulations and Pawley refinement are conducted using BIOVIA Material Studio software (Figure 3). By considering the symmetry and stoichiometry of the building blocks **1** and **2**, only one [4 + 4] rhombic topology can be reasonably modeled, and thus the eclipsed and staggered

DOI: 10.1021/acs.chemmater.8b00117
Chem. Mater. 2018, 30, 1762−1768

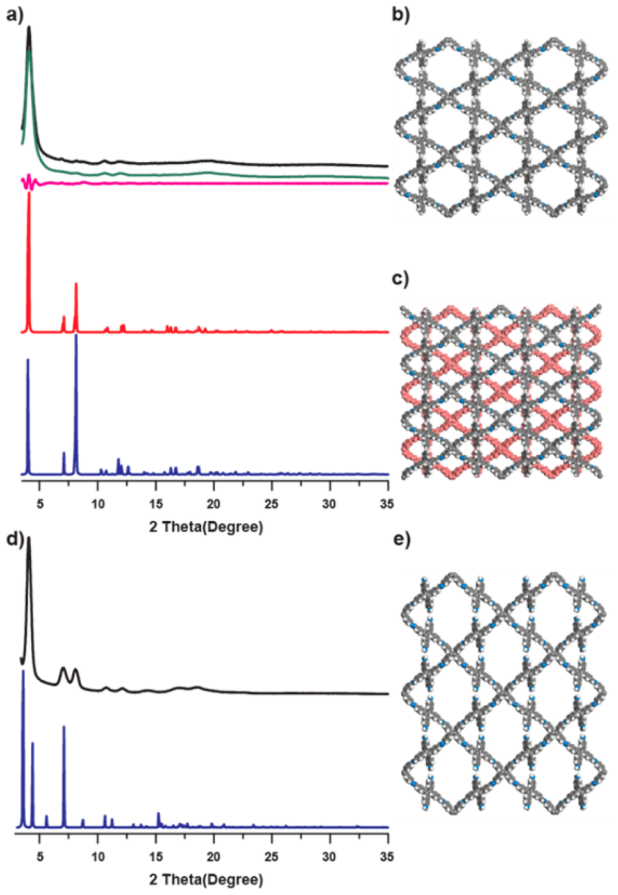

Figure 4. Powder XRD patterns of TPE-COF-III: (a) experimental (black curve), Pawley-refined (pink curve), difference between the experimental and the refined patterns (green curve), and simulated PXRD patterns for eclipsed (red curve) and staggered structure (blue curve). Simulated crystal structures of (b) eclipsed structure and (c) staggered structure. PXRD patterns of (d) experimental PXRD (black curve) and simulated PXRD patterns for eclipsed structure of TPE-COF-IV (blue curve). (e) Simulated crystal structures of the eclipsed structure of TPE-COF-IV. Views from the *c* axis. C, gray; H, white; N, blue; O, red; lower layer, pink.

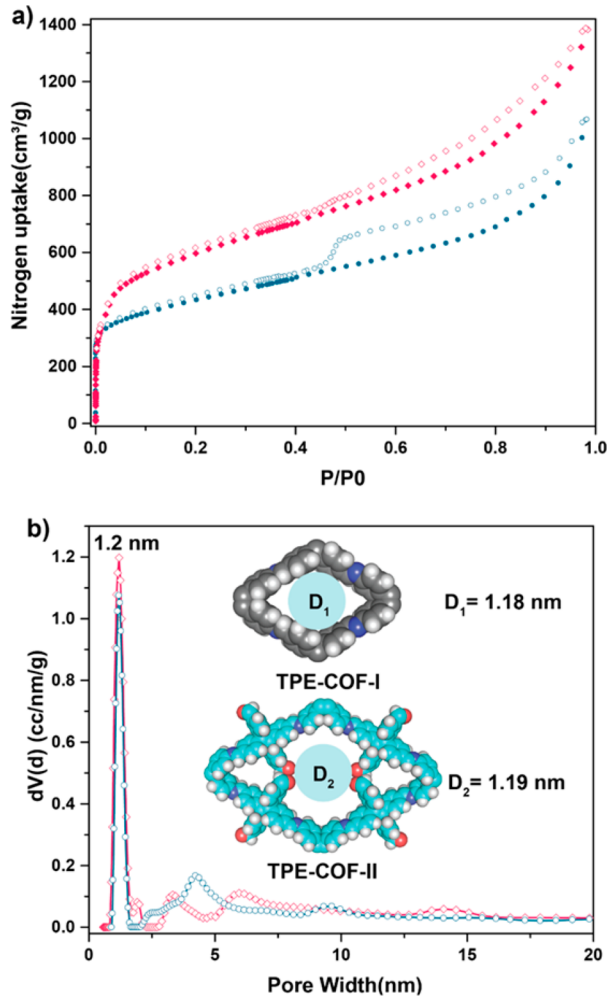

Figure 5. Nitrogen isotherms of TPE-COFs at 77 K. (a) N_2 adsorption isotherm of TPE-COF-I: adsorption (blue ●) and desorption (blue ○). N_2 adsorption isotherm of TPE-COF-II: adsorption (red ◆) and desorption (red ◇). (b) Pore size distribution of TPE-COF-I (blue ○) and TPE-COF-II (red ◇) (inset, schematic presentation of pore size).

structures are simulated based on this topology (Figure 3c,d). The obtained PXRD pattern of TPE-COF-I matches well with the simulated pattern of the eclipsed stacking structure, either in peak positions or in relative intensities (Figure 3a), suggesting that TPE-COF-I features a rhombus topology with an eclipsed stacking model. Specifically, Pawley refinement produces a monoclinic *Pm* space group with a = 20.40 Å, b = 15.70 Å; c = 5.20 Å; $\alpha = \gamma = 90°$, $\beta = 86.5°$ (R_{wp} = 2.75%, R_p = 2.09%, Table S2 in the SI).

Surprisingly, the observed PXRD patterns of TPE-COF-II do not match any of the calculated models based on the [4 + 4] rhombic topology. Only a [2 + 4] condensation product, which we named TPE-COF-II (Figure 2b), can match the experimental XRD patterns. Changing the feed ratio of **1** and **2** to a 2:1 ratio in the same solvothermal condition still generates a product with similar PXRD pattern as that of the 1:1 ratio due to the 1:1 complementary pairing needed for constructing the COF structure. This result suggests that the unusual [2 + 4] structure does not arise because of the feed ratio but is related to the nucleation dynamics which are affected by the solvents. We have simulated both the eclipsed and staggered configurations for TPE-COF-II with two *trans*-position aldehyde groups unreacted. To our delight, the simulated PXRD pattern for the eclipsed structure shows good agreement with the observed PXRD pattern of TPE-COF-II (Figure 3b,e), while the simulated PXRD patterns of the staggered structure mismatches the experimental PXRD patterns (Figure 3b,f), which excludes TPE-COF-II from the staggered stacking mode. Pawley refinements for TPE-COF-II are performed, and unit cell parameters a = 26.46 Å, b = 44.02 Å, c = 5.63 Å, $\alpha = \gamma = 90°$, $\beta = 109.9°$ (R_{wp} = 2.91% and R_p = 2.30%, Table S3 in the SI) with a monoclinic *C*2/*m* space group are obtained.

To further elucidate the crystal structure of TPE-COF-II, (*E*)-4,4′-(1,2-diphenylethene-1,2-diyl)dibenzaldehyde (*trans*-TPE-2CHO, **3**) is selected as a building unit to construct TPE-COF-III with **2**, from which only one possible structure can be formed via the [2 + 4] condensation (Figure 2c, Figure S12 in the SI). TPE-COF-III shows a similar experimental PXRD pattern as TPE-COF-II, as evidenced by similar peak positions and relative intensities (Figure S13 in the SI), thereby further confirming that TPE-COF-II adopts a similar [2 + 4] topology with two *trans*-position aldehyde groups unreacted. The simulated PXRD pattern for eclipsed structure shows good

DOI: 10.1021/acs.chemmater.8b00117
Chem. Mater. 2018, 30, 1762−1768

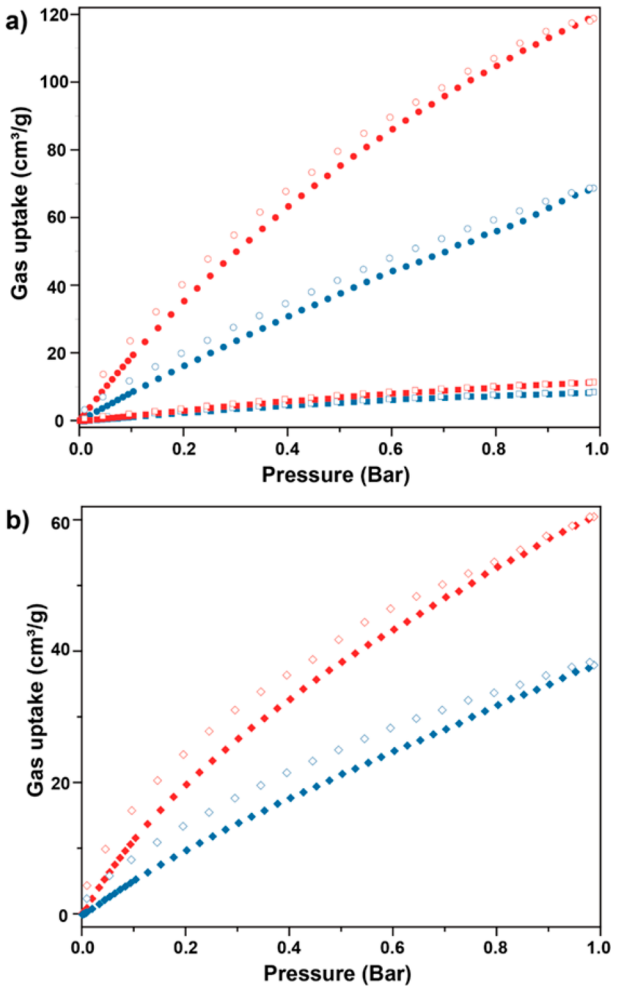

Figure 6. Gas sorption isotherms of TPE-COFs. (a) CO_2 adsorption isotherm of TPE-COF-II (red ●) and TPE-COF-I (blue ●) at 273 K; N_2 adsorption isotherm of TPE-COF-II at 273 K (red ■) and TPE-COF-I at 273 K (blue ■). (b) CO_2 adsorption isotherm of TPE-COF-II (red ◆) and TPE-COF-I (blue ◆) at 298 K.

agreement with observed PXRD pattern of TPE-COF-III (Figure 4a,b). The simulated PXRD patterns of staggered structure mismatches the experimental PXRD patterns, which excludes TPE-COF-III from the staggered structure (Figure 4a,c). In addition, the Pawley refinements for TPE-COF-III are conducted and give a monoclinic $C2/m$ space group with unit cell parameters of a = 26.33 Å, b = 44.54 Å, c = 5.65 Å, $\alpha = \gamma$ = 90°, β = 110.9° (R_{wp} = 4.41% and R_p = 3.55%, Table S4 in the SI), which are close to those of TPE-COF-II, further demonstrating that TEP-COF-II and TPE-COF-III have similar architectures with eclipsed stacking model (Figures 2b,c). Furthermore, theoretical simulation of another possible structure (TPE-COF-IV) with two *trans*-position amine groups unreacted is also conducted (Figure 4d). However, the simulated PXRD pattern does not agree with the experimental result, which excludes the possibility of TPE-COF-IV structure (Figures 4d,e and S38 and Table S5 in the SI). Thus, the structure of TPE-COF-II is confirmed as a periodic [2 + 4] COF structure with two *trans*-position aldehyde groups unreacted.

Besides the evidence from simulated crystal structure, the existence of unreacted aldehyde groups is also confirmed by FT-IR and solid-state ^{13}C CP-MAS NMR measurement. A much stronger C═O stretching vibration band (1697 cm^{-1}) is observed in the FT-IR spectrum for TPE-COF-II, compared to the other two COFs (Figure S18 in the SI). This large abundance of aldehyde groups suggests these arise not only from residues at the edges of COFs[16] but also from aldehyde groups inside the lattice of TPE-COF-II material. Solid-state ^{13}C CP-MAS NMR spectroscopy also reveals a higher intensity of a peak at 190 ppm assignable to the aldehyde groups in TPE-COF-II, as compared to the other two COFs (Figure S16 in the SI).

It is instructive to examine the structure of the framework around the vacancy to understand the origin of the different structures that resulted in the synthesis of TPE-COFs. According to the simulated crystal structure for TPE-COFs, the *cis* carbon−carbon bond angle around the olefin bond in TPE-COF-I is 115.6°, whereas it is 112.4° in TPE-COF-II, and this has an important effect on the COF growth (Figures S36a and S37a in the SI). This result is also consistent with the less rigid nature of TPE building units.[36−38] Furthermore, if we create a vacancy in TPE-COF-I by removing the TPE-4NH_2, a square-like 7.99 Å × 9.48 Å vacancy surrounded by four aldehyde groups is left behind (Figure S36b in the SI), and this is the footprint needed for a monomer to fill up the vacancy. However, the vacancy in TPE-COF II is a long rectangle of 13.39 Å × 2.73 Å (Figure S37b in the SI), which imposes a size-exclusion effect on TPE-4NH_2 monomer. Thus, the steric hindrance and mismatched symmetry (i.e., distance, angle, etc.) of TPE-COF-II structure blocks the further condensation of amine building block **2** with the unreacted aldehyde groups in TPE-COF-II, resulting in the unusual [2 + 4] pathway with the frustrated bonding network. We speculate that the choice of solvents affects the pathways toward TPE-COF-I and TPE-COF-II due to subtle differences in stacking chemistry at the initial stage of COF crystallization, although the details are not understood at this stage. It can be expected that a [2 + 4] condensation reaction would proceed faster than a [4 + 4] one since only half the bonds are needed to extend the 2D network. This has been confirmed by *ex situ* PXRD analysis of the crystallization process of TPE-COF-I and TPE-COF-II (Figures S9 and S11 in the SI).[42,43] TPE-COF-I shows low crystallinity after 2 h, while TPE-COF-II develops good crystallinity within the first hour, indicating the formation of highly crystalline TPE-COF-II is more facile than that of TPE-COF-I.

The permanent porosity of TPE-COF-I and TPE-COF-II is investigated by nitrogen sorption measurements at 77 K, after activation at 120 °C for 8 h (Figure 5). The Brunauer−Emmett−Teller (BET) surface areas of TPE-COF-I and TPE-COF-II are calculated to be 1535 and 2168 $m^2\ g^{-1}$, and their pore volumes are calculated to be 1.65 $cm^3\ g^{-1}$ (P/P_0 = 0.983) and 2.14 $cm^3\ g^{-1}$ (P/P_0 = 0.984), respectively (Figure 5a). According to pore-size calculation, there are two micro-pores sizes centered at 1.18 and 1.19 nm (Figures 5b, S22, and S24 in the SI), which agree well with the predicted pore sizes from the simulated crystal structures. Due to their permanent porosity, COFs are promising candidates for CO_2 capture and storage to mitigate the green-house effect.[32,33] Since TPE-COF-II has higher surface area and also unreacted functional groups in its lattice, it is expected to show a higher CO_2 adsorption performance than TPE-COF-I. To verify this, CO_2 adsorption analyses of TPE-COF-I and TPE-COF-II are carried out at 273 and 298 K (Figures 6 and S26−S29 in the SI). The adsorption isotherm reveals that the CO_2 uptake capability of TPE-COF-I

DOI: 10.1021/acs.chemmater.8b00117
Chem. Mater. 2018, 30, 1762−1768

is 68.6 cm^3 g^{-1} (13.4 wt %, 1 atm, 273 K) and 37.8 cm^3 g^{-1} (7.38 wt %, 1 atm, 298 K), while TPE-COF-II exhibits higher CO_2 uptake capacity at 118.8 cm^3 g^{-1} (23.2 wt %, 1 atm, 273 K) and 60.5 cm^3 g^{-1} (11.8 wt %, 1 atm, 273 K), respectively. To the best of our knowledge, the CO_2 uptake capacity observed for TPE-COF-II is among the highest reported to date for COF-based materials (see Table S6 in the SI),[8] including FCTF-1-600 (124 cm^3 g^{-1}),[13] FCTF-1(105 cm^3 g^{-1}),[13] TpPa-COF(MW) (111 cm^3 g^{-1}),[14] and COF-JLU2 (110 cm^3 g^{-1}).[15]

CONCLUSION

In summary, we have demonstrated that, using identical building units, structural variants of conventional 2D-COFs can be derived by using different solvents. Such structural variants are not predicted by conventional COF topological design rules but originate from solvent-influenced crystallization chemistry and open a new synthetic space in making framework structure with unreacted linker groups around the pores. Uniquely, the presence of a frustrated bonding network in the COF structural variant produces pores with dramatically different chemical properties as compared to the conventional COF. TPE-COF-II affords a higher surface area and higher CO_2 uptake capacity than that of TPE-COF-I. Discovering solvent-directed strategies to generate structural variants of a monostructure COF will broaden the synthetic scope for making tunable framework structures with multifunctional properties.

ASSOCIATED CONTENT

Supporting Information

The Supporting Information is available free of charge on the ACS Publications website at DOI: 10.1021/acs.chemmater.8b00117.

Additional experimental procedures, powder XRD, FT-IR, TGA, solid-state ^{13}C CP/MAS NMR, BET analysis, gas adsorption/desorption isotherms, SEM and TEM images, and structural modeling (PDF)

AUTHOR INFORMATION

Corresponding Author

*K. P. Loh. E-mail: chmlohkp@nus.edu.sg.

ORCID

Qiang Gao: 0000-0002-8783-3245
Guo-Hong Ning: 0000-0002-5640-9062
Bingbing Tian: 0000-0003-1508-6217
Wei Tang: 0000-0001-7154-4089
Kian Ping Loh: 0000-0002-1491-743X

Notes

The authors declare no competing financial interest.

Crystallograpic data for **3** in CIF format is available from the Cambridge Crystallographic Data Centre (CCDC 1585213).

ACKNOWLEDGMENTS

K.P.L. acknowledges NRF-CRP grant "Two Dimensional Covalent Organic Framework: Synthesis and Applications", Grant Number NRF-CRP16-2015-02, funded by National Research Foundation, Prime Minister's Office, Singapore. This project is also supported by Shenzhen Peacock Plan (Grant No. KQTD2016053112042971).

REFERENCES

(1) Diercks, C. S.; Yaghi, O. M. The Atom, the Molecule, and the Covalent Organic Framework. *Science* **2017**, *355*, eaal1585.
(2) Feng, X.; Ding, X.; Jiang, D. Covalent Organic Frameworks. *Chem. Soc. Rev.* **2012**, *41*, 6010−6022.
(3) Ding, S.-Y.; Wang, W. Covalent Organic Frameworks (COFs): from Design to Applications. *Chem. Soc. Rev.* **2013**, *42*, 548−568.
(4) Colson, J. W.; Dichtel, W. R. Rationally Synthesized Two-dimensional Polymers. *Nat. Chem.* **2013**, *5*, 453−465.
(5) Slater, A. G.; Cooper, A. I. Porous Materials. Function-led Design of New porous Materials. *Science* **2015**, *348*, aaa8075.
(6) Huang, N.; Wang, P.; Jiang, D. Covalent Organic Frameworks: a Materials Platform for Structural and Functional Designs. *Nat. Rev. Mater.* **2016**, *1*, 16068.
(7) Jin, Y.; Hu, Y.; Zhang, W. Tessellated Multiporous Two-dimensional Covalent Organic Frameworks. *Nat. Rev. Chem.* **2017**, *1*, 0056.
(8) Zeng, Y.; Zou, R.; Zhao, Y. Covalent Organic Frameworks for CO2 Capture. *Adv. Mater.* **2016**, *28*, 2855−2873.
(9) Zou, L.; Sun, Y.; Che, S.; Yang, X.; Wang, X.; Bosch, M.; Wang, Q.; Li, H.; Smith, M.; Yuan, S.; Perry, Z.; Zhou, H.-C. Porous Organic Polymers for Post-Combustion Carbon Capture. *Adv. Mater.* **2017**, *29*, 1700229.
(10) Huang, N.; Wang, P. M.; Addicoat, A.; Heine, T.; Jiang, D. Ionic Covalent Organic Frameworks: Design of a Charged Interface Aligned on 1D Channel Walls and Its Unusual Electrostatic Functions. *Angew. Chem., Int. Ed.* **2017**, *56*, 4982−4986.
(11) Furukawa, H.; Yaghi, O. M. Storage of Hydrogen, Methane, and Carbon Dioxide in Highly Porous Covalent Organic Frameworks for Clean Energy Applications. *J. Am. Chem. Soc.* **2009**, *131*, 8875−8883.
(12) Gao, Q.; Bai, L.; Zhang, X.; Wang, P.; Li, P.; Zeng, Y.; Zou, R.; Zhao, Y. Synthesis of Microporous Nitrogen-Rich Covalent-Organic Framework and Its Application in CO2 Capture. *Chin. J. Chem.* **2015**, *33*, 90−94.
(13) Zhao, Y.; Yao, K. X.; Teng, B.; Zhang, T.; Han, Y. A Perfluorinated Covalent Triazine-based Framework for Highly Selective and Water−tolerant CO2 Capture. *Energy Environ. Sci.* **2013**, *6*, 3684−3692.
(14) Wei, H.; Chai, S.; Hu, N.; Yang, Z.; Wei, L.; Wang, L. The Microwave-assisted Solvothermal Synthesis of a Crystalline Two-dimensional Covalent Organic Framework with High CO2 Capacity. *Chem. Commun.* **2015**, *51*, 12178−12181.
(15) Li, Z.; Zhi, Y.; Feng, X.; Ding, X.; Zou, Y.; Liu, X.; Mu, Y. An Azine-Linked Covalent Organic Framework: Synthesis, Characterization and Efficient Gas Storage. *Chem. - Eur. J.* **2015**, *21*, 12079−12084.
(16) Ding, S.-Y.; Gao, J.; Wang, Q.; Zhang, Y.; Song, W.-G.; Su, C.-Y.; Wang, W. Construction of Covalent Organic Framework for Catalysis: Pd/COF-LZU1 in Suzuki−Miyaura Coupling Reaction. *J. Am. Chem. Soc.* **2011**, *133*, 19816−19822.
(17) Lin, S.; Diercks, C. S.; Zhang, Y.-B.; Kornienko, N.; Nichols, E. M.; Zhao, Y.; Paris, A. R.; Kim, D.; Yang, P.; Yaghi, O. M.; Chang, C. J. Covalent Organic Frameworks Comprising Cobalt Porphyrins for Catalytic CO2 Reduction in Water. *Science* **2015**, *349*, 1208−1213.
(18) Xu, H.; Gao, J.; Jiang, D. Stable, Crystalline, Porous,Covalent Organic Frameworks as a Platform for Chiral Organocatalysts. *Nat. Chem.* **2015**, *7*, 905−912.
(19) Wang, X.; Han, X.; Zhang, J.; Wu, X.; Liu, Y.; Cui, Y. Homochiral 2D Porous Covalent Organic Frameworks for Heterogeneous Asymmetric Catalysis. *J. Am. Chem. Soc.* **2016**, *138*, 12332−12335.
(20) Fang, Q.; Gu, S.; Zheng, J.; Zhuang, Z.; Qiu, S.; Yan, Y. 3D Microporous Base-Functionalized Covalent Organic Frameworks for Size-Selective Catalysis. *Angew. Chem., Int. Ed.* **2014**, *53*, 2878−2882.
(21) Dalapati, S.; Jin, E.; Addicoat, M.; Heine, T.; Jiang, D. Highly Emissive Covalent Organic Frameworks. *J. Am. Chem. Soc.* **2016**, *138*, 5797−5800.
(22) Ding, S.-Y.; Dong, M.; Wang, Y.-W.; Chen, Y.-T.; Wang, H.-Z.; Su, C.-Y.; Wang, W. Thioether-Based Fluorescent Covalent Organic

DOI: 10.1021/acs.chemmater.8b00117
Chem. Mater. 2018, 30, 1762−1768

Framework for Selective Detection and Facile Removal of Mercury-(II). *J. Am. Chem. Soc.* **2016**, *138*, 3031−3037.
(23) Lin, G.; Ding, H.; Yuan, D.; Wang, B.; Wang, C. A Pyrene-Based, Fluorescent Three-Dimensional Covalent Organic Framework. *J. Am. Chem. Soc.* **2016**, *138*, 3302−3305.
(24) Ning, G.-H.; Chen, Z.; Gao, Q.; Tang, W.; Chen, Z.; Liu, C.; Tian, B.; Li, X.; Loh, K. P. Salicylideneanilines-Based Covalent Organic Frameworks as Chemoselective Molecular Sieves. *J. Am. Chem. Soc.* **2017**, *139*, 8897−8904.
(25) Kandambeth, S.; Biswal, B. P.; Chaudhari, H. D.; Rout, K. C.; Kunjattu H., S.; Mitra, H. S.; Karak, S.; Das, A.; Mukherjee, R.; Kharul, U. K.; Banerjee, R. Selective Molecular Sieving in Self-Standing Porous Covalent-Organic-Framework Membranes. *Adv. Mater.* **2017**, *29*, 1603945.
(26) Fang, Q.; Wang, J.; Gu, S.; Kaspar, R. B.; Zhuang, Z.; Zheng, J.; Guo, H.; Qiu, S.; Yan, Y. 3D Porous Crystalline Polyimide Covalent Organic Frameworks for Drug Delivery. *J. Am. Chem. Soc.* **2015**, *137*, 8352−8355.
(27) Bai, L.; Phua, S. Z. F.; Lim, W. Q.; Jana, A.; Luo, Z.; Tham, H. P.; Zhao, L.; Gao, Q.; Zhao, Y. Nanoscale Covalent Organic Frameworks as Smart Carriers for Drug Delivery. *Chem. Commun.* **2016**, *52*, 4128−4131.
(28) DeBlase, C. R.; Silberstein, K. E.; Truong, T.-T.; Abruña, H. D.; Dichtel, W. R. *β*-Ketoenamine-Linked Covalent Organic Frameworks Capable of Pseudocapacitive Energy Storage. *J. Am. Chem. Soc.* **2013**, *135*, 16821−16824.
(29) Liu, W.; Luo, X.; Bao, Y.; Liu, Y. P.; Ning, G.-H.; Abdelwahab, I.; Li, L.; Nai, C. T.; Hu, Z. G.; Zhao, D.; Liu, B.; Quek, S. Y.; Loh, K. P. A Two-dimensional Conjugated Aromatic Polymer via C−C Coupling Reaction. *Nat. Chem.* **2017**, *9*, 563−570.
(30) Feng, X.; Chen, L.; Honsho, Y.; Saengsawang, O.; Liu, L.; Wang, L.; Saeki, A.; Irle, S.; Seki, S.; Dong, Y.; Jiang, D. An Ambipolar Conducting Covalent Organic Framework with Self-Sorted and Periodic Electron Donor-Acceptor Ordering. *Adv. Mater.* **2012**, *24*, 3026−3031.
(31) Lin, C.-Y.; Zhang, L.; Zhao, Z.; Xia, Z. H. Design Principles for Covalent Organic Frameworks as Efficient Electrocatalysts in Clean Energy Conversion and Green Oxidizer Production. *Adv. Mater.* **2017**, *29*, 1606635.
(32) Leung, D. Y. C.; Caramanna, G.; Maroto-Valer, M. M. An Overview of Current Status of Carbon Dioxide Capture and Storage Technologies. *Renewable Sustainable Energy Rev.* **2014**, *39*, 426−443.
(33) D'Alessandro, D. M.; Smit, B.; Long, J. R. Carbon Dioxide Capture: Prospects for New Materials. *Angew. Chem., Int. Ed.* **2010**, *49*, 6058−6082.
(34) Furukawa, H.; Cordova, K. E.; O'Keeffe, M.; Yaghi, O. M. The Chemistry and Applications of Metal-Organic Frameworks. *Science* **2013**, *341*, 1230444.
(35) Stock, N.; Biswas, S. Synthesis of Metal-Organic Frameworks (MOFs): Routes to Various MOF Topologies, Morphologies, and Composites. *Chem. Rev.* **2012**, *112*, 933−969.
(36) Qin, A.; Tang, B. Z. *Aggregation-Induced Emission: Fundamentals*; Wiley-VCH: New York, 2013.
(37) Mei, J.; Leung, N. L. C.; Kwok, R. T. K.; Lam, J. W. Y.; Tang, B. Z. Aggregation-Induced Emission: Together We Shine, United We Soar! *Chem. Rev.* **2015**, *115*, 11718−11940.
(38) Yang, Z.; Qin, W.; Leung, N. L. C.; Arseneault, M.; Lam, J. W. Y.; Liang, G.; Sung, H. H. Y.; Williams, I. D.; Tang, B. Z. A Mechanistic Study of AIE Processes of TPE Luminogens: Intramolecular Rotation vs. Configurational Isomerization. *J. Mater. Chem. C* **2016**, *4*, 99−107.
(39) Zhou, T.-Y.; Xu, S.-Q.; Wen, Q.; Pang, Z.-F.; Zhao, X. One-Step Construction of Two Different Kinds of Pores in a 2D Covalent Organic Framework. *J. Am. Chem. Soc.* **2014**, *136*, 15885−15888.
(40) Ascherl, L.; Sick, T.; Margraf, J. T.; Lapidus, S. H.; Calik, M.; Hettstedt, C.; Karaghiosoff, K.; Döblinger, M.; Clark, T.; Chapman, K. W.; Auras, F.; Bein, T. Molecular Docking Sites Designed for the Generation of Highly Crystalline Covalent Organic Frameworks. *Nat. Chem.* **2016**, *8*, 310−316.
(41) Pang, Z.-F.; Xu, S.-Q.; Zhou, T.-Y.; Liang, R.-R.; Zhan, T.-G.; Zhao, X. Construction of Covalent Organic Frameworks Bearing Three Different Kinds of Pores through the Heterostructural Mixed Linker Strategy. *J. Am. Chem. Soc.* **2016**, *138*, 4710−4713.
(42) Smith, B. J.; Overholts, A. C.; Hwang, N.; Dichtel, W. R. Insight into the Crystallization of Amorphous Imine-linked Polymer Networks to 2D Covalent Organic Frameworks. *Chem. Commun.* **2016**, *52*, 3690−3693.
(43) Gao, Q.; Bai, L.; Zeng, Y.; Wang, P.; Zhang, X.; Zou, R.; Zhao, Y. Reconstruction of Covalent Organic Frameworks by Dynamic Equilibrium. *Chem. - Eur. J.* **2015**, *21*, 16818−16822.

DOI: 10.1021/acs.chemmater.8b00117
Chem. Mater. 2018, 30, 1762−1768